Synthesis and characterization of mesoporous silicas with dendritic and spongy-like structures: potential supports for human lactate dehydrogenase-based microreactors

Microporous and Mesoporous Materials 376 (2024) 113182

Contents lists available at ScienceDirect

Microporous and Mesoporous Materials

journal homepage: www.elsevier.com/locate/micromeso

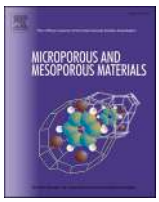

Synthesis and characterization of mesoporous silicas with dendritic and spongy-like structures: Potential supports for human lactate dehydrogenase-based microreactors aimed at anticancer inhibitor screening

Clarissa Cocuzza [a], Chiara Vincenzi [a], Carminna Ottone [b], Andrés Illanes [b], Debora Fino [a], Valentina Cauda [a], Marco Piumetti [a,*]

[a] Department of Applied Science and Technology, Politecnico di Torino, Corso Duca Degli Abruzzi, 24, 10129, Turin, Italy
[b] Escuela de Ingeniería Bioquímica, Pontificia Universidad Católica de Valparaíso, Av. Brasil 2085, Valparaíso, Chile

ARTICLE INFO

Keywords:
Spongy-like supports
Dendritic mesoporous silica
Multipoint covalent immobilization
LDH-A enzyme
Biosensor

ABSTRACT

Mesoporous silica are versatile materials with wide-ranging potential. Notably, they excel as enzyme supports. This work examines the influence of three distinct siliceous mesoporous materials used as supports for the enzyme human lactate dehydrogenase (*h*LDH-A). Drugs with inhibition effects have recently shown favorable effects on diminishing the proliferation of cancerous cells. The ultimate goal of this research is to produce a stable and effective biocatalyst suitable for being employed in a microreactor for the screening of *h*LDH-A inhibitors. The synthesized mesoporous silica exhibited distinctive structural features, including a quasi-mesocellular network, bent-channels structure, and a dendritic geometry with radial symmetry, as evidenced by FESEM and HR-TEM. These materials were functionalized with amino and aldehyde groups to covalently immobilize *h*LDH-A. Characterization of both pristine and functionalized materials involved a comprehensive examination of their physico-chemical properties. The CO dosing revealed Brønsted acidity characteristic of mesoporous silica, while FT-IR spectroscopy and N_2 physisorption at 77 K confirmed their successful functionalization. Enzyme immobilization on the functionalized supports, performed with stabilizing agents such as PEG (0.05 mg mL^{-1}) or trehalose (300 mM), produced promising results. The immobilization yield consistently exceeded 80 %, with retained activity reaching values as high as 15 %. The immobilization of the enzyme on mesoporous silica increased the stability of *h*LDH-A against alkaline and organic solutions. These findings hold significance for those exploring siliceous porous supports for enzyme immobilization, paving the way for the development of stable and active biocatalysts.

1. Introduction

In light of the survey conducted by the International Agency for Research on Cancer (IARC), which projects a surge in new cancer cases to reach 30.2 million by 2040, understanding the metabolic pathways of cancer cells becomes crucial [1]. Aerobic glycolysis is the metabolic pathway common to cancerous cells of different tissues, such as lung, bronchus, colorectal, breast, prostate, tracheal, and pancreatic [2]. In these cells, the isoform A of the enzyme lactate dehydrogenase (*h*LDH-A) is overexpressed. *h*LDH-A preferentially converts pyruvate into lactate; in cancerous cells this reaction is carried out even in aerobic conditions, producing an accumulation of lactate which acts as a signaling molecule that makes aerobic glycolysis to proceed [3,4]. Recent studies have shown that inhibiting *h*LDH-A can diminish the proliferation of cancerous cells, this treatment presents fewer severe side effects than conventional chemotherapy [5–7]. Moreover, the inhibition of lactate dehydrogenase can increase the sensitivity of cancer to traditional chemotherapeutic agents [5,6].

Despite significant advancements in biotechnology and medicine, searching for new compounds with chemotherapeutic properties remains a persistent challenge. Indeed, discovering new anticancer drugs is both time-consuming and financially demanding due to the several

* Corresponding author.
E-mail address: marco.piumetti@polito.it (M. Piumetti).

https://doi.org/10.1016/j.micromeso.2024.113182
Received 23 February 2024; Received in revised form 27 April 2024; Accepted 17 May 2024
Available online 18 May 2024
1387-1811/

thousands of compounds that are usually tested, typically requiring an average of 12 years and USD 2.7 billion for the development of each new drug [8,9]. The construction of a device that can test different compounds speeding up the screening phase and allowing the recovery of the enzyme could reduce the overall cost of the process [10,11]. In this scenario, electrochemical sensors are gaining interest due to their several benefits. In fact, their cost is lower than traditional analytical methods (such as spectroscopy, chromatography, or electrophoresis), they are easy to use, specific, and selective, they allow real-time on-sight measurements, and their sensitivity towards biomolecule detection [12]. Tvorynska et al. [13] suggested the possibility of building up an amperometric sensor constituted of two different sections: a miniature bioreactor, composed in this case of *h*LDH-A immobilized on an inorganic support and an amperometric sensing device.

This research aims to evaluate the effectiveness of different mesoporous silica used as support for *h*LDH-A with the purpose of realizing a stable microreactor unit for the aforementioned amperometric biosensor that could be employed for the screening of *h*LDH-A inhibitors. Extensive literature has been dedicated to the utilization of mesoporous silica as a support for covalent immobilization of enzymes [14–19]. Indeed, ordered mesoporous silica, including SBA-15, MCM-41, and MCF, among others, exhibit notable characteristics, such as high specific surface areas, substantial pore volumes, and tunable pores [20–22]. These materials showcase chemical stability in aqueous environments and offer the flexibility of morphology adjustment [23]. In fact, by modifying the synthesis parameters and the precursors involved, different geometry of the inorganic network can be obtained. Moreover, a swelling agent can be added to the previously mentioned solution to increase the dimension of the pores [14,22]. Another advantage of mesoporous silica is the possibility of being activated post-synthesis with almost any functional group, a fundamental property to attach enzymes permanently [23,24]. Among various immobilization strategies proposed over time, irreversible methods proved to be more suitable than reversible ones for achieving a stable and enduring biocatalyst. Specifically, covalent binding appears as the most appropriate because it provides minimal enzyme leakage and potentially higher stabilization [25].

In this work, three mesoporous silicas have been prepared to be used as supports for the immobilization of lactate dehydrogenase (LDH). Indeed, a mesocellular foam (MCF) structure, a SBA-15-like material (mSBA-15), and a silica with dendritic topology (DPS) were chosen for this study. In particular, MCF and mSBA-15 were selected because their pores size is generally between 5 and 40 nm (5–15 nm for SBA-15 and 15–40 nm for MCF), and this could enhance the enzyme loading and stability of the immobilized enzyme [26,27]. Additionally, the synthesis method for the SBA-15-inspired material was refined to mitigate limitations associated with its one-dimensional cylindrical pore structure, namely addressing enzyme diffusion challenges and mass transfer constraints for large molecules [28]. On the other hand, dendritic particle silica, have recently received attention as enzyme carriers due to their radial porous structure featuring expansive pore openings [28]. The utilization of materials with diverse textural and structural characteristics enables the exploration of how the support's features affect the immobilized enzyme. The three materials have been functionalized with amino and aldehyde groups in order to perform the covalent immobilization of *h*LDH-A. The pristine and functionalized materials have been characterized with different techniques to gain knowledge about their chemical and physical properties. The enzyme was immobilized on the functionalized mesoporous silica via multipoint covalent attachment in the presence of two different stabilizing agents (polyethylene glycol and trehalose). For the sake of brevity, the result of the best immobilization procedure, hereafter referred to as imm-*h*LDH-A, was further analyzed. This analysis aimed to acquire data on the stabilization effect provided by the support and to assess the feasibility of employing imm-*h*LDH-A in a microreactor for evaluating lactate dehydrogenase inhibition.

2. Materials and methods

2.1. Materials

1,2,3-trimethylbenzene (TMB or mesitylene), Pluronic P-123, tetraethyl orthosilicate (TEOS), urea, hexadecyltrimethylammonium bromide (CTAB), (3-glycidyloxypropyl)trimethoxysilane (GPTMS), (3-Aminopropyl)triethoxysilane (APTES), sulfuric acid, hydrochloric acid (37 % wt.), polyethylene glycol (PEG), toluene, acetone, $CuSO_4$, KH_2PO_4, K_2HPO_4, $NaHCO_3$, Na_2CO_3, H_2NaO_4P, Na_2HPO_4, 1-hydroxy-6-phenyl-4-(trifluoromethyl)-1H-indole-2-carboxylic acid methyl ester (NHI-2), dimethylsulfoxide (DMSO), and L-lactate dehydrogenase from human expressed in *Escherichia. coli* (*h*LDH-A, EC 1.1.1.27) were supplied by Sigma-Aldrich (Merck). Potassium iodide, glutaraldehyde (50 % in water solution), sodium meta periodate, lactic acid, sodium pyruvate, sodium borohydride, and NADH were purchased from VWR Avantor.

2.2. Methods

2.2.1. Synthesis of the mesoporous silica

MCF (*mesocellular silica foams*) was synthesized using a direct hydrothermal synthesis method previously reported by Pietricola et al. [18] and Piumetti et al. [20]: 4 g of P-123 (templating agent) was added to 1.6 M HCl solution (150 mL). The solution was kept at 40 °C under vigorous stirring until a homogeneous solution was obtained. Subsequently, 3 g of mesitylene (swelling agent) and 8.5 g of tetraethyl orthosilicate (TEOS) were added drop-wise to guarantee a good dispersion of the components. The solution was stirred at 40 °C for 24 h for nucleation to occur. The suspension obtained was transferred into a Teflon autoclave to be hydrothermally treated at 100 °C for 24 h. The suspension was separated by centrifugation, washed several times with ethanol and MilliQ water, and dried at 60 °C overnight. The obtained powder was calcined at 550 °C for 5 h (heating ramp equal to 45 °C/h).

A modified SBA-15 material (hereafter referred to as mSBA-15) was prepared following the same procedure adopted for mesostructured silica-type materials [18], modifying the ratio between the reagents: 3.75 g of P-123 (templating agent) was added to 2 M HCl solution (150 mL). Then 0.94 g of mesitylene (swelling agent) and 7.97 g of tetraethyl orthosilicate (TEOS) were added drop-wise. A swelling/templating agents ratio different from the traditional one was used to increase the pore diameters [27].

DPS (*Dendritic Particle Silica*) was synthesized by adapting the heterogeneous oil−water biphase method previously reported [29]. 8 mL of TEOS were added to 63 mL of butanol solution (5 % v/v) in cyclohexane, and the solution was vigorously stirred at room temperature. 5.6 g of CTAB were added to a urea solution (2 % w/w.) and vigorously stirred at room temperature. When a homogeneous CTAB solution was obtained, it was poured into TEOS solution and vigorously stirred at room temperature for 30 min. The suspension obtained was transferred into a Teflon autoclave to be hydrothermally treated at 130 °C for 5 h. The suspension was separated by centrifugation, washed several times with ethanol and MilliQ water, and dried at 60 °C overnight. The powder obtained was calcined at 550 °C for 5 h (heating ramp equal to 45 °C/h).

2.2.2. Silica functionalization

The mesoporous silica were functionalized to provide amino and glyoxyl groups with a three-step procedure, adapting the method previously reported by Cocuzza et al. [2]. 1 g of mesoporous silica was added to 30 mL of APTES and GPTMS solution (APTES 5 % v/v and GPTMS 5 % v/v in ethanol) and strongly stirred at room temperature for 5 h. The first step provided the amino and epoxy groups. The epoxy groups were hydrolyzed to diols in the second phase during which the material obtained (1 g) was put in contact with 0.1 M H_2SO_4 (30 mL) and vigorously stirred for 2 h at 85 °C. During the last step, the modified mesoporous silica (1 g) was put in contact with 0.1 M $NaIO_4$ (30 mL) and

vigorously stirred for 2 h at room temperature. In this phase, the diols were oxidized to obtain glyoxyl groups. At the end of each step, the support was separated by centrifugation, washed with acetone and abundant MilliQ water, and dried at room temperature. The glyoxyl groups on the silica surface were quantified through the back-titration method with $NaHCO_3$/KI [30]. The moles of glyoxyl groups were determined by Equation (1):

$$\frac{mol_{gly}}{m_{sup}} = \frac{1}{m_{sup}} \cdot V_{IO_4^-} \cdot \left[IO_4^-\right]_{in} \cdot \left(1 - \frac{Abs_f}{Abs_0}\right) \quad (1)$$

where mol_{gly} are the moles of glyoxyl groups (mmol), m_{sup} is the amount of functionalized silica support (g), $V_{IO_4^-}$ is the volume of metaperiodate solution (mL), $[IO_4^-]$ is the concentration of IO_4^- ions in the $NaIO_4$ solution (mmol mL^{-1}), and Abs_0 and Abs_f are the values of absorbance measured at 420 nm, for the supernatant at the beginning and the end of the reaction, respectively. The number of amino groups grafted on the support surface were evaluated through the interaction between $CuSO_4$ and $–NH_2$ [2]. The moles of amino groups were determined by Equation (2):

$$\frac{mol_{NH2}}{m_{sup}} = \frac{1}{m_{sup}} \cdot V_{CuSO_4} \cdot \left[CuSO_4\right]_{in} \cdot \left(1 - \frac{Abs_f}{Abs_0}\right) \quad (2)$$

where mol_{NH2} are the moles of amino groups (mmol), m_{sup} is the amount of functionalized silica support (g), V_{CuSO_4} is the volume of $CuSO_4$ solution (mL), $[CuSO_4]$ is the concentration of $CuSO_4$ (mmol mL^{-1}), and Abs_0 and Abs_f are the values of absorbance measured at 750 nm.

2.2.3. Materials characterization

The morphology of the synthesized mesoporous silica was investigated through high-resolution field emission scanning electron microscopy (ZEISS Merlin® FE-SEM equipped with a Gemini-II column, operating at 3 kV).

The structure of the samples was investigated through high-resolution transmission electron microscopy (HR-TEM, Talos Thermo Scientific, LaB_6 gun, operating at 200 kV). The powder was dispersed in isopropanol and deposited on copper grids equipped with Lacey Carbon films.

The pristine and functionalized MCF, mSBA-15, and DPS were analyzed by N_2 physisorption at −196 °C with Micromeritics ASAP TriStar II 3020 instrument, after pretreatment at 200 °C, atmospheric pressure in N_2 atmosphere for 2 h. The specific surface areas (S_{BET}) were calculated by applying the Brunauer-Emmet-Teller method, the micropore volumes were evaluated by applying the Barrett-Joyner-Halenda (V_p) approach to the adsorption phase.

Powder X-ray diffractograms of the synthesized and functionalized samples were acquired with EMPYREAN diffractometer, Cu Kα radiation, angle step size 0.013. MCF and mSBA-15 were analyzed in the 2θ range of 0.2°–5° in the presence of a divergence slit fixed of 0.38 mm. DPS was analyzed in the 2θ range of 10°–50° in the presence of a divergence slit fixed of 0.76 mm. The diffractograms were examined using the Powder Data File Databases (PDF-2 Release 2004, COD_Mar10).

The synthesized and functionalized mesoporous silica were inspected through Fourier transform IR (FT-IR) spectroscopy with Bruker INVENIO instrument equipped with liquid nitrogen cooled MCT detector. The samples were pretreated at 150 °C and 300 °C in standard vacuum conditions for 1 h the analyses were performed at room temperature (range 4000–400 cm^{-1}, 64 scans, resolution 4 cm^{-1}).

In order to study the chemical properties, and in particular the acidity of the silica, the samples were outgassed at 150 °C for 1 h, before dosing probe molecules (CO and NH_3). The CO was dosed from 0.001 to 20 mbar keeping the sample at −196 °C, and finally, the reversibility of the interaction was evaluated [21]. The acidity can be connected with the hydroxyl population, which is involved in the formation of the covalent bonds with the organosilanes. The results are displayed as normalized difference spectra, obtained by subtracting the corresponding spectra of the bare sample. To obtain information on the chemical properties of the surface of the supports on which the enzyme will be immobilized, and in particular, to evaluate the nature of the acidic sites present, ammonia was dosed from 0.01 to 20 mbar at room temperature, because it interacts more strongly than CO [31,32]. The reversible fraction of the NH_3 adsorbed was then removed by prolonged evacuation. The results are displayed as normalized difference spectra, obtained by subtracting the corresponding spectra of the bare sample.

The instrument Zetasizer Nano ZS90 (Malvern Panalytical) was used to inspect the ζ-potential of the functionalized silica in the immobilization conditions since it is a key physical parameter for gaining insights into the immobilization mechanisms. The functionalized silica were dispersed in 25 mM carbonate buffer pH 9, with 0.05 mg mL^{-1} PEG or 300 mM trehalose, resulting in a final concentration of 200 μg mL^{-1}, the reported value is an average of three measurements.

2.2.4. Characterization of LDH-A and activity assays

As previously mentioned, the synthesized mesoporous silica were used as supports *h*LDH-A from human expressed in *E. coli* (UniProt ID. K1T0A2) hereafter referred to as *h*LDH-A. UniProt database reports a molecular weight equal to 27.46 kDa for this enzyme. Consequently, its minimum diameter, estimated by applying Equation (3) [33], is 3.98 nm.

$$D_{min} = 2 \bullet \left(0.066 \bullet \sqrt[3]{M}\right) \quad (3)$$

where D_{min} is the minimum diameter of the enzyme whose shape is approximated to a sphere (nm) while M is the molecular weight of the enzyme (Da).

The activity tests were performed in a UV-VIS spectrophotometer (Jasco V-730) by monitoring for 60 s the decrease in absorbance at 340 nm, which corresponds to the peak of NADH. The absorbance variation in time (ΔA) is directly proportional to the specific activity of the biocatalyst. The specific activity of the free (A_{FE}, U mg_{prot}^{-1}) was calculated using Equation (4).

$$A_{FE} = \frac{\Delta A}{\varepsilon L} \cdot \frac{V_s}{V_e} \cdot \frac{1}{c_e} \quad (4)$$

where ΔA is the absorbance slope, ε is the NADH molar extinction coefficient (6.22 mM^{-1} cm^{-1}), L is the optical path (cm), V_s is the volume of the solution in the cuvette (mL), V_e is the volume of enzymatic solution (mL), and c_e is the concentration of the enzymatic solution (mg mL^{-1}), respectively. To perform the test, a solution (2.9 mL) of 0.24 mM of NADH and 1.69 mM of pyruvate in 0.1 M phosphate buffer pH 7.5 was used as blank, then 100 μL of *h*LDH-A solution (0.01 mg mL^{-1}) were added to the blank solution and the reacting system was kept at 35 °C. A_{FE} of the free *h*LDH-A was 407.9 ± 16.1 U mg_{prot}^{-1}. The specific activity of imm-*h*LDH-A (A_{IE}, U g_{supp}^{-1}) was calculated using Equation (4) after applying the proper modifications: V_e is the volume (mL) and c_e is the concentration (g mL^{-1}) of the imm-*h*LDH-A suspension. To perform the test, 100 μL of imm-*h*LDH-A suspension (20 mg mL^{-1}) were added to the blank solution.

2.2.5. Immobilization

The functionalized supports prepared were used to immobilize *h*LDH-A following the procedure previously reported by Cocuzza et al. [2]. The immobilization was carried out by incubating the enzyme with the functionalized support in an alkaline environment that is required to deprotonate the lysine residues and to allow them to react with the aldehyde groups present on the support surface [25]. The immobilization process was conducted at pH 9 instead of pH 10, despite the pKa of lysine being at pH 10 [34], due to the tendency of the protein to denature in a more alkaline environment. At pH 9 the 9 % of ε-amino groups

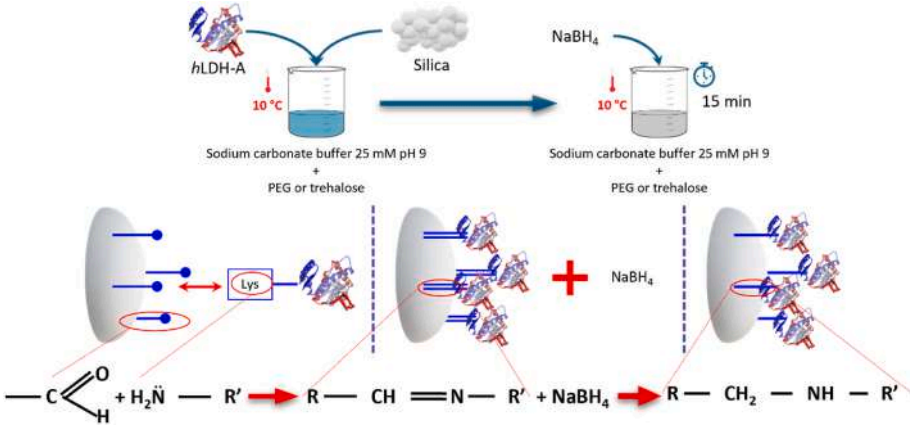

Fig. 1. Scheme of the immobilization procedure adopted to attach hLDH-A to silica surface. 47.

of lysine is estimated to be in ε-NH_2 form, and the overall charge of the enzyme is positive [35]. The immobilization was accomplished in the presence of additives to improve the enzyme's stability and to protect it from the alkaline environment [36]. In particular, PEG at a concentration of 0.05 mg mL^{-1} or 300 mM trehalose was used. 1 mg of *h*LDH-A was adjoined to 1 g of functionalized mesoporous silica in 40 mL of 25 mM carbonate buffer pH 9 (with PEG or trehalose in the proper amounts). The resultant mixture was maintained at 10 °C under gentle agitation. Fig. 1 presents a scheme of the immobilization procedure. Regularly, samples were collected to monitor the activity of the supernatant and to check that the enzyme was not inactivated by the immobilization conditions [37]. This was carried out by monitoring the activity of the suspension and the activity of an enzymatic solution, which was kept at the same conditions as the immobilizing mixture but not in contact with the support. When the supernatant activity dropped to zero or remained constant for two consecutive samplings, the Schiff' bases created between the enzyme and the support were reduced in a sodium borohydride solution (0.1 mg mL^{-1} in 100 mL of 25 mM carbonate buffer pH 9 with PEG) for 15 min. Subsequently, the resulting mixture was subjected to vacuum filtration and rinsed with a 25 mM phosphate buffer at pH 7.5. A sample of the filtered solution was collected to monitor if the phosphate buffer washed away the enzyme. Finally, the imm-*h*LDH-A was washed with MilliQ water and dried at a temperature of 4 °C.

To assess the immobilization yield (IY), which quantifies the amount of protein attached to the support surface, the activity of the solution was determined at the beginning (A_{LDH,t_0}) and at the end (A_{LDH,t_f}) of the immobilization process, as expressed in Equation (5) [36].

$$IY\ (\%) = \frac{A_{LDH,t_0} - A_{LDH,t_f}}{A_{LDH,t_0}} \cdot 100 \quad (5)$$

The efficiency of the imm-*h*LDH-A was valued according to its retained activity (R_{act}). R_{act} was determined as the ratio between the specific activity of the imm-*h*LDH-A and the specific activity of the free enzyme multiplied by the enzymatic load used in the immobilization, as expressed in Equation (6) [30]:

$$R_{act}\ (\%) = \frac{A_{IE}}{q \cdot A_{FE}} \cdot 100 \quad (6)$$

where A_{IE} is the specific activity of the immobilized *h*LDH-A (U g_{sup}^{-1}), q is the enzymatic load provided during the immobilization ($mg_{prot}\ g_{sup}^{-1}$), and A_{FE} is the specific activity of the free *h*LDH-A (U mg_{prot}^{-1}).

2.2.6. Characterization of the immobilized enzyme

With the aim of obtaining information about the covalent bonds formed between the enzyme and the support, FT-IR spectra were acquired on the functionalized silica and compared with the spectra acquired with *h*LDH-A immobilized on the supports with the two different stabilizing agents. The IR spectra were acquired with Bruker INVENIO instrument equipped with liquid nitrogen cooled MCT detector. The samples were degassed to 10^{-3} mbar and the analyses were performed at room temperature (range 4000–400 cm^{-1}, 64 scans, resolution 4 cm^{-1}).

Optical fluorescence microscopy was performed to obtain information about the enzyme presence and its distribution on the support; for the sake of brevity, the analysis was performed only following the immobilization procedure that gave the best results in terms of R_{act} and IY. With this purpose, *h*LDH-A was labeled with ATTO 550 fluorescence dye. To label the enzyme, the procedure provided by the manufacturer (Merck) was followed, as previously employed by Rocha-Martín et al. [38] The enzyme solution was incubated with ATTO 550 at room temperature in 0.1 M sodium bicarbonate buffer pH 9.5 for 2 h, the mixture was protected from light and kept under gentle stirring, and finally, it was separated with a gel filtration column (PD-10). The labeled enzyme was then immobilized according to the immobilization procedure previously described, avoiding the contact with light. The imm-*h*LDH-A obtained was observed with a Nikon Eclipse Ti-e fluorescence optical inverted microscope, equipped with a super bright wide-spectrum source (Shutter Lambda XL), a high-resolution camera (Zyla 4.2 Plus, 4098 × 3264 pixels, Andor Technology), and an objective 100× (Nikon) suitable for oil immersion. Brightfield, green, and blue emission images were acquired. The support was observed as a control at the same conditions of analysis.

With the purpose of obtaining information concerning the stability of *h*LDH-A in the free and immobilized forms, enzymatic assays were performed on the enzymatic solution and the best imm-*h*LDH-A suspension both incubated at pH 10 or 30 % v/v ethanol (in 0.1 M phosphate buffer pH 7.5) at room temperature for 3 h. The test was then performed at pH 7.5.

2.2.7. Inhibition tests

Enzymatic activity tests varying the concentration of NADH and pyruvate were performed on the free and the immobilized *h*LDH-A. These tests were carried out in the presence and the absence of the well-known inhibitor NHI-2 to obtain information about the inhibition achieved on the immobilized *h*LDH-A compared with its free form. The pyruvate concentration was varied in the range from 0.05 to 1 mM, keeping constant the concentration of the cofactor at 0.23 mM. The NADH concentration was varied in the range from 0.05 to 0.4 mM keeping the substrate pyruvate at its saturating concentration (1.63 mM). As previously stated, these tests were repeated in the presence of the inhibitor by the addition of 20 μL of 3.02 mM NHI-2 diluted in DMSO. Each data point was triplicated and represented as the mean of the acquired values for the Lineweaver-Burk linearization fitting.

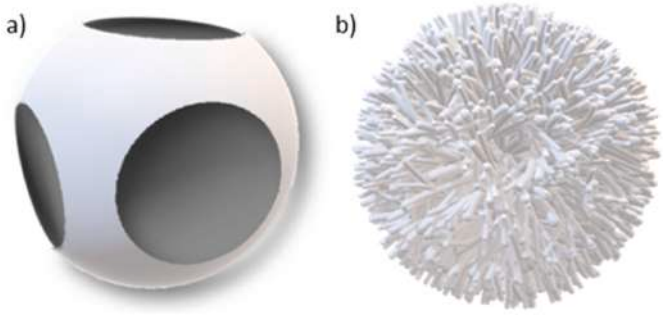

Fig. 2. Schematization of sponge-like (a) and dendritic (b) structures. 48.

Interpolation lines were computed and outcomes were validated using Origin 2018.

3. Results and discussion

3.1. Mesoporous silica characterization

Three different mesoporous siliceous materials were prepared as *h*LDH-A supports. MCF and mSBA-15 structures could be associated to a sponge; the assumed schematic minimal unit of these materials is shown in Fig. 2a. On the other hand, DPS should present a more ordered and regular configuration with a dendritic development and a radial symmetry; the assumed schematic minimal unit of this material is shown in Fig. 2b.

The FE-SEM images acquired on the synthesized mesoporous silica are reported in Fig. 3 to display the morphology of the prepared samples. MCF support (Fig. 3a) exhibited a sponge-like structure [18]. The detectable round structure diameters measured 3–4.5 μm and were sintered to form much bigger conglomerates. Also, the structure of the mSBA-15 support (Fig. 3b) appeared to be more sponge-like rather than having the usual ordered hexagonal appearance. This is due to the higher TMB/P-123 ratio used to expand the porosity [27]. The round structures were smaller than that of MCF with a size range from 0.7 to 1.9 μm. Otherwise, the DPS support (Fig. 3c) presents smaller spherical particles (size range: 100–200 nm) with radial symmetry, as can be seen in the magnification [29].

Fig. 4 depicts the HR-TEM images acquired on the prepared siliceous supports. As previously suggested by FESEM images, MCF (Fig. 4a) presented a disordered structure due to the TMB/P123 ratio equal to 0.75. The appearance suggests that pores have a hybrid structure between channels and mesocellular sponge, in accordance with what was previously reported by Zhou et al. [27]. Likewise, due to swelling/directing agent ratio, mSBA-15 (Fig. 4b) displayed bent channels oriented in perpendicular and longitudinal directions [27]. The image acquired on DPS (Fig. 4c) confirms the spherical shape of the particles, and especially the center-radial mesopore channels distributed along the three spatial directions [28,29].

The powder X-ray diffractogram acquired on DPS agrees with what was previously reported by Chen et al. [29]. However, the XRD of mSBA-15 and MCF did not exhibit the well-defined reflection peaks typical of mesoporous silica due to the absence of a long-range order structure, in accordance with TEM images [39]. Fig. S1 of the Supporting Information shows the powder X-ray diffractograms of the pristine silica.

The functionalization method adopted proved to be effective across all mesoporous silica; therefore, all the supports prepared have a

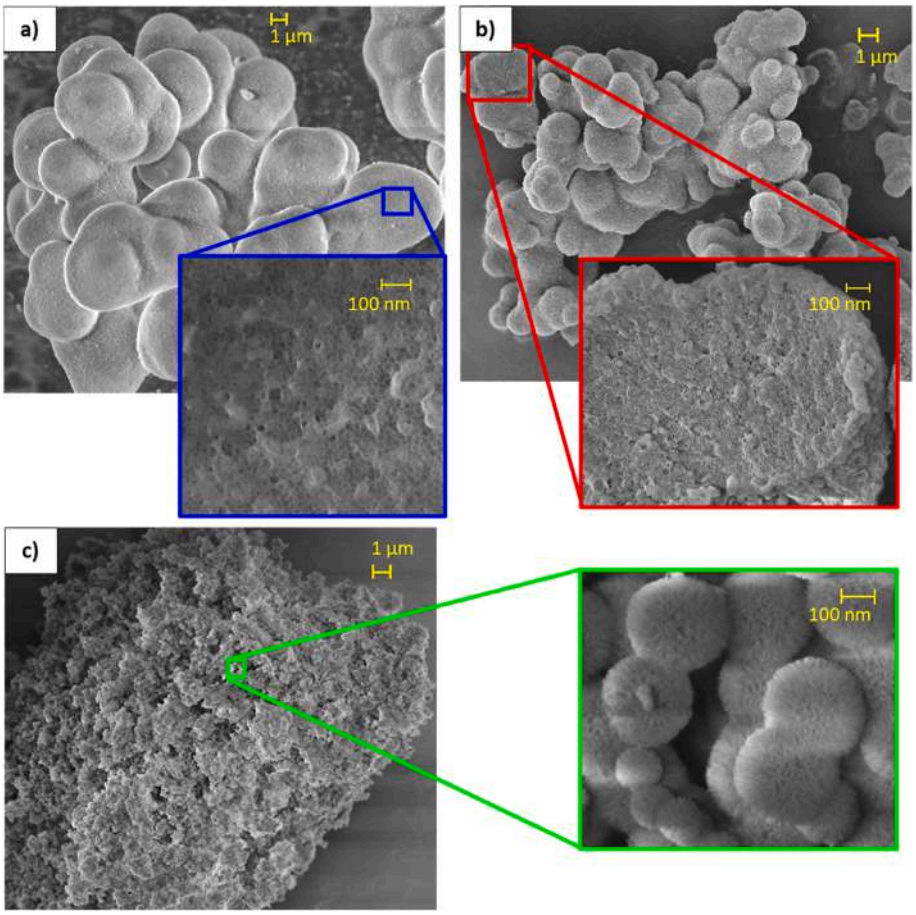

Fig. 3. FE-SEM images acquired on a) MCF, b) mSBA-15, and c) DPS, along with their magnifications. 49.

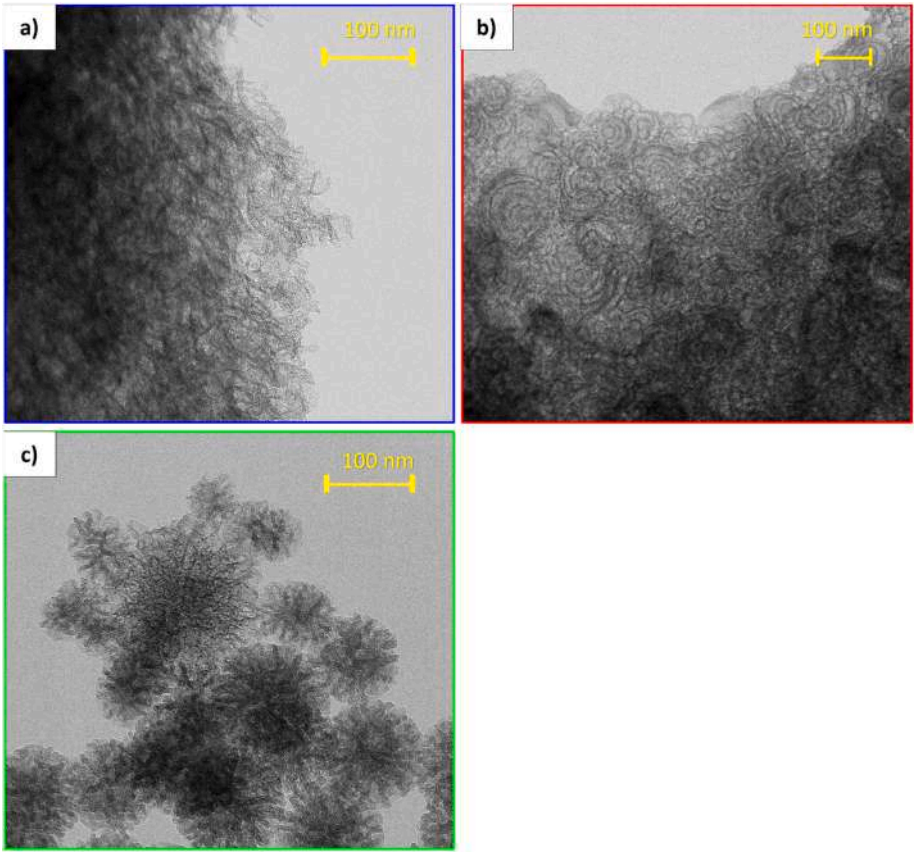

Fig. 4. HR-TEM images acquired on a) MCF, b) mSBA-15, and c) DPS, along with their magnifications. 50.

Table 1
Quantification of glyoxyl and amino groups obtained after the functionalization process performed on the silica supports.

Support	Glyoxyl groups (mmol g^{-1})	Amino groups (mmol g^{-1})
MCF	0.70 ± 0.09	1.55 ± 0.01
mSBA-15	1.01 ± 0.05	1.30 ± 0.01
DPS	1.18 ± 0.02	1.09 ± 0.01

quantity of both amino and glyoxyl groups in the order of 1 mmol g^{-1}, Table 1 reports in detail the amount of amino and glyoxyl groups obtained. Significantly, the material with an average content of both amino and glyoxyl groups exhibits intermediate values of Brønsted acidity, as evidenced by the CO dosing (*vide infra*). The acidity of the silanols present in the support plays a key role in the attachment of organosilanes to the surface of silica [40].

Fig. 5 shows the N_2 physisorption isotherms and pore size distribution (dV/dD_{pore}) collected on pristine and functionalized supports. MCF and mSBA-15 displayed type IVa isotherms, according to the IUPAC classification, which is typical of mesoporous materials. Particularly, MCF and mSBA-15 exhibited type IVa isotherms due to the presence of a hysteresis loop caused by condensation. Concerning the hysteresis loops, both MCF and mSBA-15 are characterized by type H2 attributed to material with complex pores arrangement such as networks with ink-bottle shape pores [41]. Specifically, the H2b hysteresis loop can be associated with MCF while the H2a loop can be related to mSBA-15 [41]. By contrast, DPS revealed an almost completely reversible type II isotherms, suggesting the absence of significant mesopores the adsorbate distribution (Fig. 5) describes the amount of volume condensed in slit-like nanospaces [42].

As a result of the functionalization process, the specific surface area decreased by ~50 % for all the studied materials, specifically: 47 % for MCF, 55 % for mSBA-15, and 34 % for DPS. An analogous trend is evident for the cumulative adsorbed pore volume too, as can be observed in Table 2. These outcomes can be a consequence of the occlusion of the smaller pores by APTES and GPTMS, as previously reported [43,44].

FT-IR spectra, displayed in Fig. 6 were acquired on functionalized and non-functionalized mesoporous silica to inspect thoroughly the chemical modifications in the support surface as a result of the functionalization process. In the region from 4000 to 2500 cm^{-1}, all the pristine supports pretreated at 150 °C for 1 h presented isolated (3743 cm^{-1}), vicinal (3710 cm^{-1}), and geminal (3530 cm^{-1}) silanols absorption bands. Fig. S2 of the Supporting Information shows a scheme of the different silanols [45]. These signal intensities were significantly lower or absent in the spectra of the functionalized silica, due to the formation of bonds between the silanols of silica and the organosilanes molecules. The absorption bands at 3405 cm^{-1}, and around 2900 cm^{-1}, visible in the functionalized supports, are the results of the functionalization process and can be ascribed to -NH and $–CH_2$ vibrations respectively. The absorption bands correlated to the silanols and –NH vibrations were significantly reduced after the outgassing at 300 °C [21]. The peaks of lower intensity around 2900 cm^{-1} identified in the unfunctionalized spectra can be related to alkyl groups (CH_2, CH_3) [46,47].

The effect of the functionalization is particularly apparent in the region 2200–1340 cm^{-1}, where numerous absorption bands correlated to –CO and –NH vibrations emerged in the functionalized silica spectra. The intensities of the absorption peaks correlated to carbonyl and alkyl groups decrease after the outgassing at 300 °C. Table 3 reports a complete list of the absorption peaks identified in functionalized and non-functionalized silica spectra.

As previously stated, FT-IR spectra recorded on CO adsorption allow to study the strength of acid sites [55]. Fig. 7 displays the normalized difference spectra acquired on the three pristine supports outgassed at

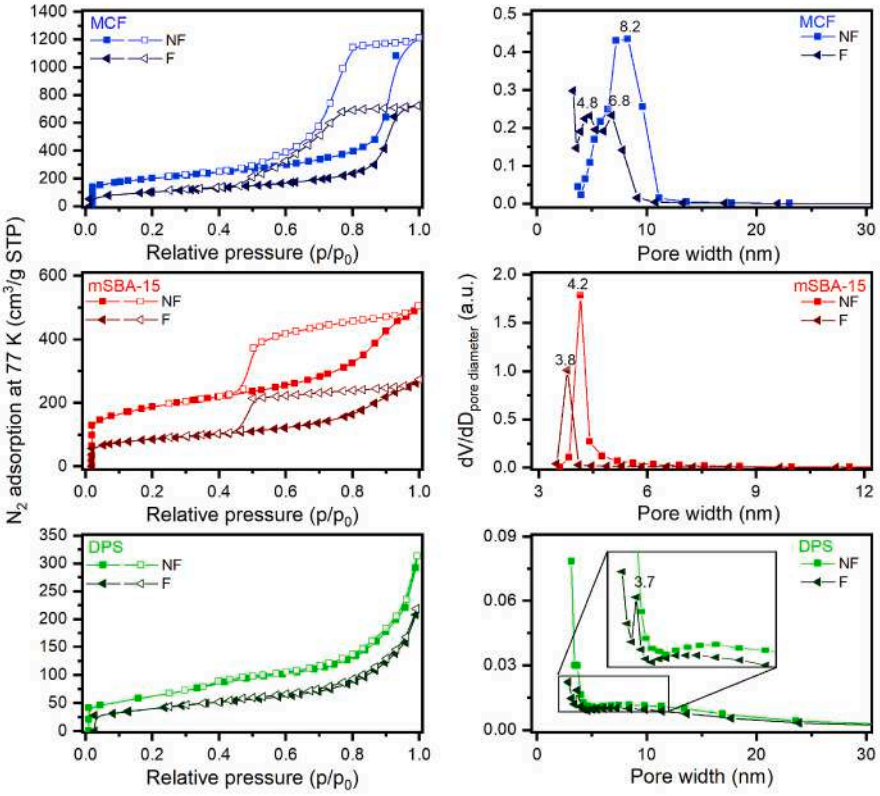

Fig. 5. N_2 physisorption isotherms at −196 °C (left) and pore size distributions (right) of pristine (NF) and functionalized (F) mesoporous silica. 51.

Table 2
Textural properties of functionalized (F) and non-functionalized (NF) MCF, mSBA-15, and DPS materials.

Support	S_{BET} ($m^2\ g^{-1}$)[a]	V_p ($cm^3\ g^{-1}$)[b]	D_p (nm)[c]
MCF_NF	691	1.6	8.2
MCF_F	369	1.1	4.8; 6.8
mSBA-15_NF	673	0.6	4.2
mSBA-15_F	301	0.3	3.8
DPS_NF	224	0.4	–
DPS_F	147	0.3	3.7

[a] Specific surface area calculated through the BET method.
[b] Cumulative adsorbed pore volume calculated through the BJH method.
[c] Pore diameter.

150 °C as the result of CO dosage. The CO absorption is perfectly reversible as demonstrated by the expansions in Fig. S3 of the Supporting Information. Moreover, the adsorption of CO molecules on mesoporous silica was confirmed by the presence of three distinct peaks visible in the insets in Fig. 7. The peak at 2110 cm^{-1} is correlated to the CO coordinated to the SiOHs through its oxygen atom [55], the band at 2138 cm^{-1} is due to CO condensed on the silica surface, and the signal at 2157 cm^{-1} is ascribed to CO adsorbed onto the mildly acidic silanol groups [56]. Two negative signals can be observed in the silanols region (3800–3000 cm^{-1}), whereas two new absorption bands appeared at lower wavenumbers. The negative bands are the result of the interaction between CO and the hydroxyl of the silanols through hydrogen bonding, those originally absorbing at 3742–3740 cm^{-1} (isolated silanols) shifted to 3636–3610 cm^{-1} while those initially absorbing at 3715–3713 cm^{-1} (vicinal silanols) shifted to 3463–3424 cm^{-1}. The calculated red-shift ($\Delta\nu$) between the negative and positive band of a specific type of silanols is a measure of the Brønsted acidity of the related hydroxyls: the larger the $\Delta\nu$, the more acidic are the hydroxyls [21,31,32]. Table 4 reports the red-shift measured for the isolated and terminals silanols of the pristine MCF, mSBA-15, and DPS.

The red-shifts listed in Table 4, suggest that the acidity is higher for vicinal than isolated silanols for all supports. In particular, the Brønsted acidity order seems to be: MCF > mSBA-15 > DPS. The average acidity observed in mSBA-15 may be caused by an optimal balance between the quantity and acidic strength of its silanol groups. In order to study how functionalization changes the samples' acidity, the CO dosage was carried out on functionalized mSBA-15. Fig. S4 of the Supporting Information displays the comparison between pristine and functionalized silica after CO dosage. The silica's acidity was reduced after the functionalization step, as evidenced by the lower intensities of the subtracted spectra and by the intensity of the peaks in the inset. In fact, in contrast to the spectra of pristine mSBA-15, the functionalized material presented an absorption peak at 2138 cm^{-1} with higher intensity than that at 2157 cm^{-1}, suggesting that the CO mainly condensed on the sample.

Ammonia was dosed on functionalized silica to analyze the chemical properties of the surfaces of the supports on which the enzyme will be immobilized. As previously reported by Piumetti et al., ammonia allowed to discriminate between Brønsted and Lewis sites, by the formation of ammonium ions or Lewis acid-base adducts, respectively [31]. Fig. 8 displays the subtracted spectra obtained by the interaction of ammonia with the functionalized silica. The absorption of ammonia causes three negative bands, two in the case of mSBA-15, (3740–3505 cm^{-1}) due to NH_3 interacting with different hydroxyl species. Accordingly, this caused a broad intense peak at 2920 cm^{-1} [31,32]. The absorption peak at about 3390–3370 cm^{-1} may be assigned to the asymmetric stretch vibrations of N–H groups of the ammonia molecule [31]. The range at the lower wavenumbers exhibited a peak at about 1641 cm^{-1} ascribable to acid-base adducts (Lewis sites) and a peak at about 1461 cm^{-1} ascribable to NH_4^+ (Brønsted sites) [31,32,46]. The smoothed absorption band at about 1560 cm^{-1} may correspond to the signal from deprotonated functional groups, where the hydrogen ions (H^+) were removed by NH_3. The ammonia absorption was not

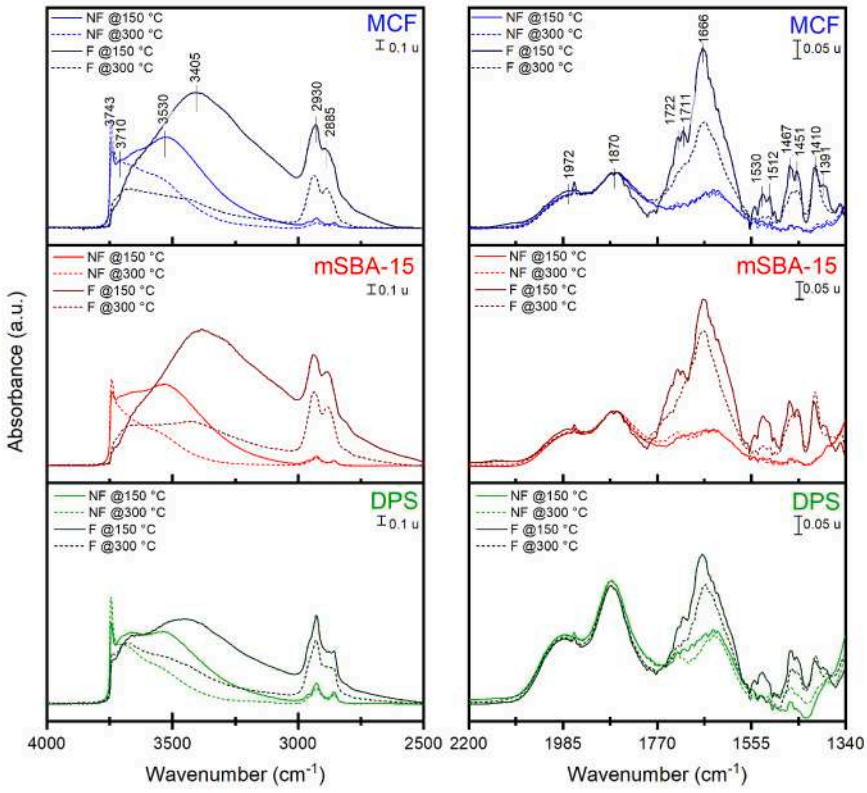

Fig. 6. FT-IR spectra of the silanols region (4000–2500 cm^{-1}) and the functional groups region (2200–1340 cm^{-1}) of functionalized (F) and non-functionalized (NF) silica pretreated at 150 °C (solid line) and 300 °C (dash line) in standard vacuum conditions for 1 h 52.

Table 3
Absorption peaks for functionalized and non-functionalized MCF, mSBA-15, and DPS.

Vibrational features	Wavenumber (cm^{-1})	Reference
Isolated silanols	3743	[2,21]
Vicinal silanols	3710	[21]
Geminal silanols	3530	[21]
Hydrogen bonding between $–NH_2$ and silanols	3405	[2]
Symmetric and asymmetric stretching $–CH_2$	2930, 2885	[2,30]
Overtones and combination of silica framework	1972, 1870	[48]
Stretching –C═O	1722	[49]
Stretching –C(=O)–OH	1711	[50]
Bending $–C(=O)–NH_2$	1666	[51]
Stretching modes $-Si-NH_2$	1530	[31]
Bending –NH	1512	[50]
Bending $–CH_3$	1470, 1451	[52]
Vibration $-Si-CH_2$	1410	[53]
Bending –CH	1391	[50]
Vibration –CN	1354	[54]

completely reversible for all the examined samples, as shown by the bold line in Fig. 8. The functionalized silica showed a very similar acidity. However, the higher intensity of the absorption bands of functionalized mSBA-15 suggests a slightly higher acid nature.

Fig. 9 shows the ζ-potential calculated for functionalized silica dispersed in 25 mM carbonate buffer pH 9, with 0.05 mg mL^{-1} PEG or 300 mM trehalose. As previously reported, the functionalized silica had a negative ζ-potential when measured in an alkaline environment (pH 9), probably due to the deprotonation of residual silanols or the functional groups [57,58].

3.2. Immobilization and characterization of lactate dehydrogenase

The functionalized mesoporous silica were used as supports to immobilize *h*LDH-A through a multipoint covalent attachment, as previously described in section 2.2.5. Fig. 10 summarizes the results obtained from the immobilizations on the three different supports in the presence of the two additives previously mentioned. Fig. S5 of the Support Information shows the immobilization parameters (the activity of the suspension, the activity of the supernatant, and the activity of the control enzymatic solution) measured as a function of time, in the tested immobilizations. Moreover, a study concerning enzyme immobilization on the pristine supports has been carried out by monitoring the activity of the supernatant of an enzymatic solution put in contact with the unfunctionalized silica at the same conditions of the immobilization protocol previously described. IYs exceeded 70 %, with values higher than 98 % in most cases. Despite this, the retained activity of the *h*LDH-A immobilized on the unfunctionalized silica is zero. These results suggest enzyme adsorption on the silica surface due to secondary interactions (electrostatics, hydrogen bonding, and van der Waals forces) [59].

As previously stated the alkaline environment can provoke the instability of the soluble enzyme, the use of stabilizing agents, such as ethylene glycol, polyethylene glycol, trehalose, dextran, can improve the enzyme stability during the immobilization [34]. As easily deduced from Fig. 10, the specific activity of the imm-*h*LDH-A is higher for all supports when the enzyme is immobilized in the presence of trehalose, an organic osmolyte which has been observed to provide protection to different proteins. In this context, while the exact stabilization mechanism remains unclear, previous studies have proposed that the cumulative interactions between amino acid side chains and osmolytes may promote protein unfolding. Conversely, unfavorable interactions between the enzyme and the osmolyte could potentially induce an overall stabilization effect [60]. Moreover, as depicted in Fig. 9, the ζ-potential

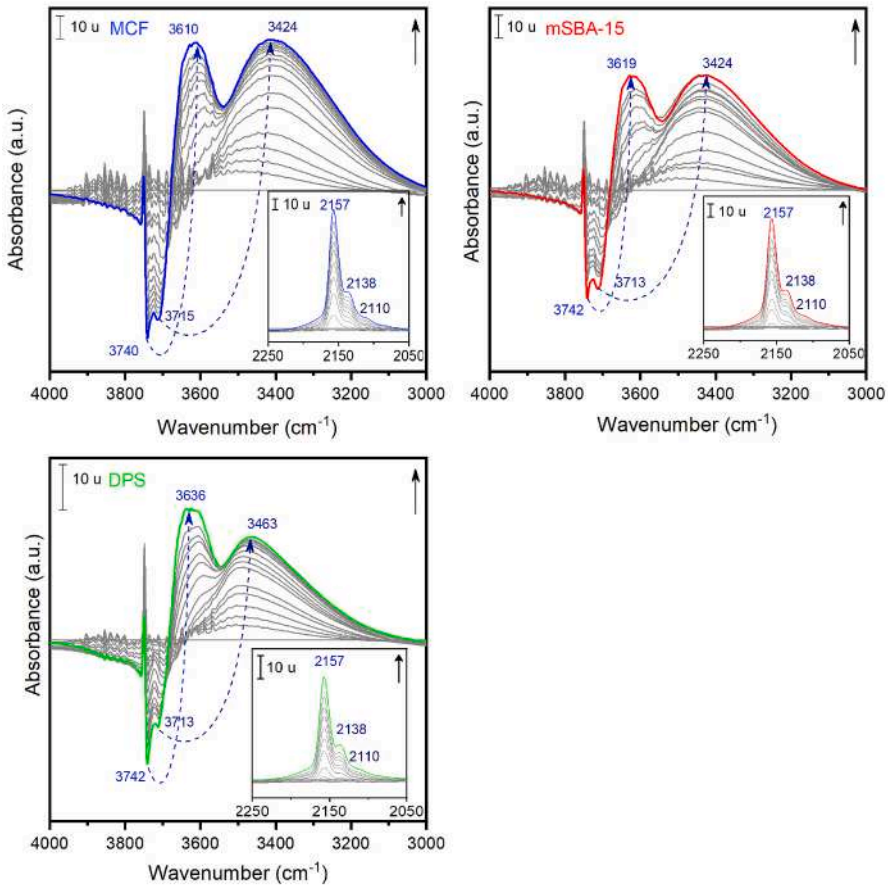

Fig. 7. FT-IR difference spectra (4000 - 3000 cm^{-1}), recorded on the pristine MCF, mSBA-15, and DPS (outgassed at 150 °C) after dosing CO (0.001–20 mbar range) at −196 °C. The insets show the CO stretching region (2250 - 2050 cm^{-1}). The bold line represents the subtracted spectra obtained at the highest CO pressure. 53.

Table 4
Red-shifts calculated for isolated and vicinal silanols on pristine MCF, mSBA-15, and DPS (outgassed at 150 °C for 1 h) after CO dosing at −196 °C.

Support	$\Delta\nu_{isolated\ silanols}$ (cm^{-1})	$\Delta\nu_{vicinal\ silanols}$ (cm^{-1})
MCF	130	297
mSBA-15	123	289
DPS	106	250

of all the functionalized supports shifted toward less negative values when trehalose was used as a stabilizing agent, consequently reducing the repulsive charges between the enzyme and the support surface [35]. In accordance with the previous statement, the best results were achieved when mSBA-15 was used as support in the presence of PEG or trehalose, being mSBA-15 the support with the less negative ζ-potential in both cases. A possible explanation can be sought in the morphology and structure of this material [61]. The morphology of DPS can affect the conformation of the enzyme. In addition, functionalized mSBA-15 support has a pore diameter lower than MCF (see Table 2 for further details), which can provoke the presence of the enzyme on the external surface of the support or in the outer section of the pores, reducing the substrate diffusion-related problems [62]. In fact, due to the small size of the studied enzyme, it could be immobilized both inside or on the outer part of the pores and on the surface of the materials. In particular, *h*LDH-A can be immobilized more easily inside the pores when MCF is used as support due to its higher mean pore diameter (4.8 nm and 6.8 nm) than mSBA-15 (3.8 nm). On the other hand, as regards to the MCF support, the interconnected tridimensional pore system can provoke substrate diffusion related problems, as previously suggested. Specific activity similar to that obtained for mSBA-15 (~62 U g^{-1}) was previously observed for *h*LDH-A immobilized on commercial MCM-41 (~52 U g^{-1}) [2]. MCM-41 was functionalized with APTES and GPTMS (both in 5 % v/v in toluene) and the immobilization was conducted by incubating the enzyme and the functionalized support in 25 mM carbonate buffer pH 9 in the presence of 0.05 mg mL^{-1} of PEG. Both mSBA-15 and MCM-41 possess similar pore diameters (3.8 nm and 3.9 nm respectively), suggesting the key role of this parameter in achieving an active immobilized enzyme.

The number of functional groups can also play a role. mSBA-15 has intermediate values of both amino and aldehyde groups (see Table 1), the former could provide an effective electrostatic interaction that can bring the protein closer to the support, while the glyoxyl groups guarantee the correct stabilization avoiding the protein stiffening that could be obtained with a greater amount of covalent bonds formed between the support and the enzyme [11].

The covalent bond established between the enzyme and the support was investigated using FT-IR measurements. Fig. 11 displays the region 2120–1370 cm^{-1} of the IR spectra acquired on the immobilized *h*LDH-A in the presence of PEG or trehalose comparing it with the corresponding functionalized mesoporous silica. The spectra acquired on the immobilized enzyme exhibited a characteristic peak at 1600 cm^{-1}, not present in the spectra of the functionalized silica, that can be associated with the stretching signal of amide I (general formula R–C(=O)-NR'R″) [63]. Conversely, the peak (1710 cm^{-1}) correlated to –CH_2-C(=O)- stretching [50,64], in the functionalized silica spectra disappeared after enzyme immobilization. The absence of the carbonyl group signal suggests that these functional groups are involved in the covalent bonds between the enzyme and the support. In fact, when a multipoint covalent

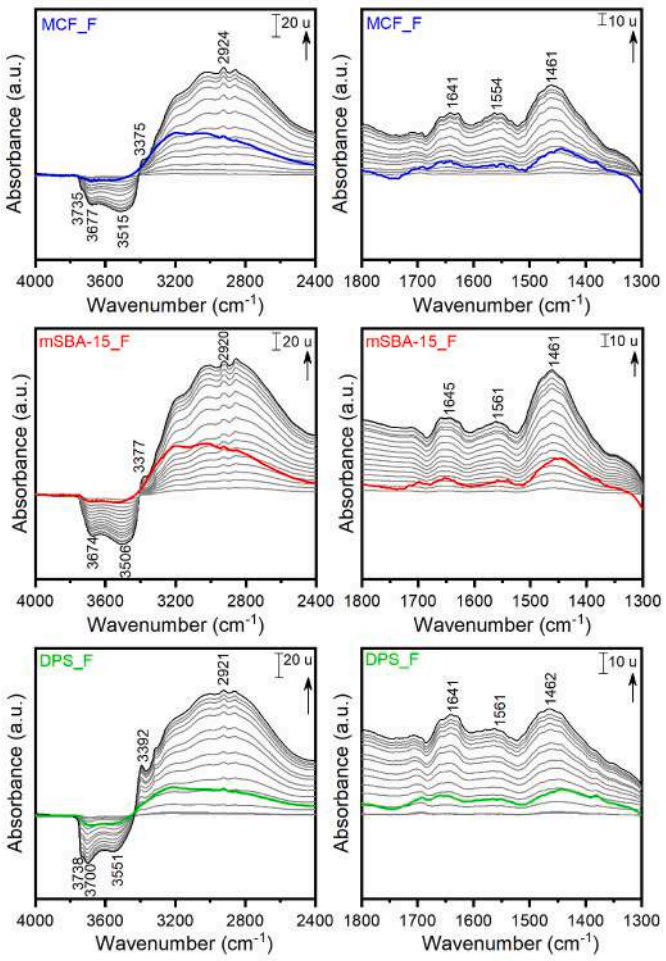

Fig. 8. FT-IR difference spectra of the silanols region (4000 - 2400 cm^{-1}) and ammonia interacting region (1800 - 1300 cm^{-1}) recorded on the functionalized MCF, mSBA-15, and DPS (outgassed at 150 °C) after dosing NH_3 (0.01–20 mbar range) at room temperature. The bold line represents the subtracted spectra obtained at the lowest pressure of the evacuation step. 54.

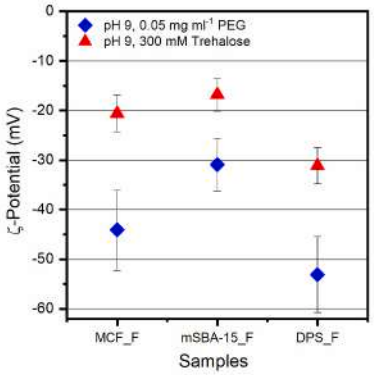

Fig. 9. ζ-potential measured for functionalized MCF, mSBA-15, and DPS suspended in 25 mM carbonate buffer pH 9 with 0.05 mg mL^{-1} PEG (◆) or 300 mM trehalose (▲). 55.

immobilization is performed under alkaline conditions, the aldehyde groups of the support react with the ε-NH_2 group of the lysine residue of the enzyme forming a Schiff' base which can be subsequently stabilized through the interaction with $NaBH_4$ [25].

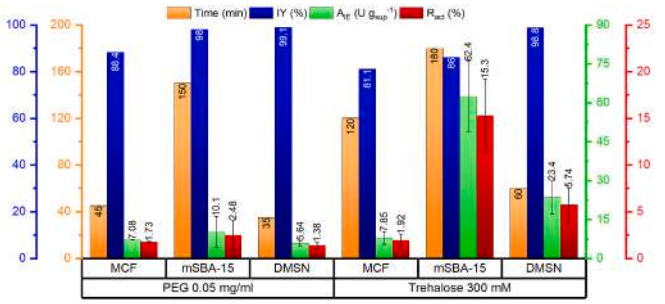

Fig. 10. Immobilization Yield (IY), specific activities (A_{IE}), and retained activity (R_{act}) achieved for the immobilized hLDH-A in the presence of PEG or trehalose. 56.

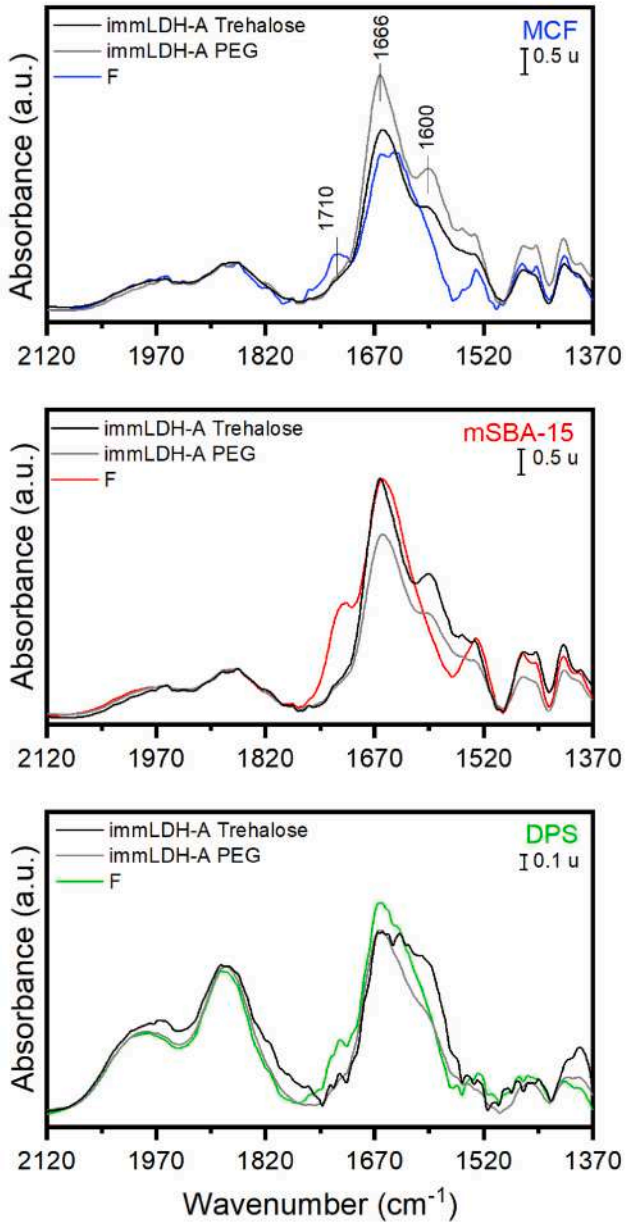

Fig. 11. Functionalized supports and imm-hLDH-A (obtained in the presence of PEG and trehalose) FT-IR spectra (region 2120–1370 cm^{-1}) collected in vacuum conditions at room temperature. 57.

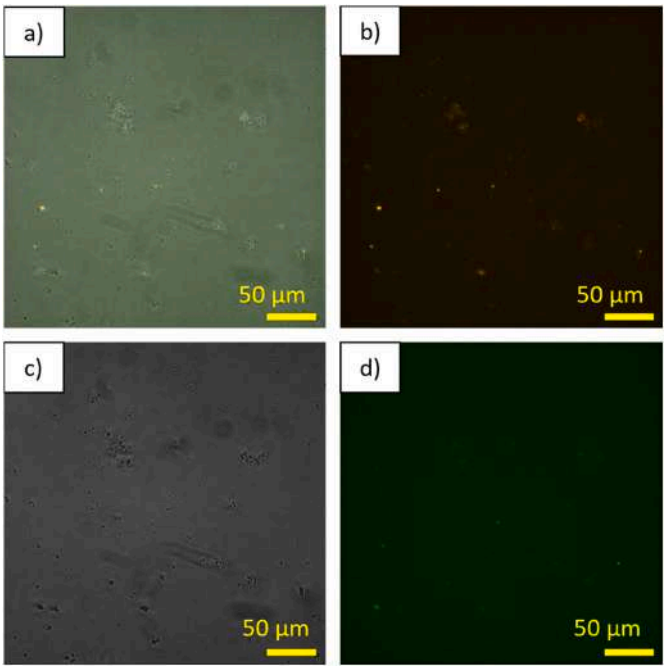

Fig. 12. Optical fluorescence microscopy images of hLDH-A labeled with ATTO 550 immobilized on mSBA-15 in the merged red and green channels (a), red channel (b), brightfield (c), and green channel (d)2. The brightness and contrast of the images were corrected. 58.

As previously stated, fluorescence microscopy was performed on *h*LDH-A immobilized on mSBA-15 to obtain information concerning the presence and distribution of the enzyme on the support. The same analysis was repeated on the bare functionalized silica (Fig. S6 of the Supporting Information) to analyze its intrinsic fluorescence phenomena. The support itself had a slight emission in the green channel and a negligible emission in the blue channel; for this reason, the latter is not reported for the imm-*h*LDH-A. Otherwise, the support had no emissions in the red channel. Fig. 12 shows the optical fluorescence microscopy images acquired on *h*LDH-A immobilized on mSBA-15.

The enzyme is recognizable as red spots, clearly visible in Fig. 12a and b, and located in correspondence with the silica particles, distinguishable in Fig. 12c and d as green spots. Although this analysis does not allow the differentiation of individual enzyme molecules due to the low magnifications, it affirms the enzyme's presence on the support after the immobilization.

The stability of both the free and immobilized forms of the prepared biocatalyst was tested in an organic solvent and at alkaline pH, considering that the biocatalyst would be used in a microreactor for screening different inhibitors, which could potentially alter the reaction media. Acidic environments were not tested since *h*LDH-A has previously shown higher activity in acidic pH compared to alkaline pH [2]. The biocatalyst activity was periodically tested after incubation in 30 % v/v ethanol solution and in 0.1 M carbonate buffer pH 10. The outcomes obtained are visible in Fig. 13 as expected, the multipoint covalent attachment on mesoporous silica support increased the stability of the enzyme [65]. Specifically, the residual activity measured for the immobilized enzyme was approximately 20 % and 35 % after the incubation in ethanol (Fig. 13a) and carbonate buffer pH 10 (Fig. 13b), respectively. By contrast, the residual activity of the free enzyme dropped to zero after 5 min. The support's nature may enhance the stability effect of immobilization. A further examination of the buffering properties of silica can be found in the Supporting Information. Earlier studies have shown that the surface of mesoporous silica can create a buffered environment with a pH around neutrality (within the pH range from 6 to 8). Moreover, it has been suggested that silica surface can produce an aqueous environment in its proximity when put in organic solvents/water mixtures [14].

3.3. Inhibition tests

To further analyze the behavior of imm-*h*LDH-A as a microreactor for the screening of chemotherapy drugs, explorative activity tests were carried out on free and immobilized forms of the enzyme, in the presence of the *h*LDH-A inhibitor NHI-2. In the case of imm-*h*LDH-A, only the apparent kinetics parameters can be directly derived due to microenvironmental effects, like mass transfer limitations and partition of substrates, caused by the immobilization which changes the enzyme phase [66]. The internal diffusional restrictions can be assessed and conveniently expressed through the effectiveness factor (η). The effectiveness factor can be calculated in terms of observable parameters, as reported by Bahamondes et al. [67] and for a Michaelis-Menten kinetics it can be determined through Equation (7):

$$\eta = \frac{(1+\beta_0)\times r_{obs}}{V_M \times \beta_0} \tag{7}$$

Where β_0 is the dimensionless substrate concentration calculated as the ratio between the molar concentration of the substrate (mM) and the intrinsic Michaelis-Menten constant (mM) [66], r_{obs} is the reaction rate observed for each substrate (or cofactor) concentration (µmol min^{-1} mg^{-1}), and V_M is the maximum rate obtained for the enzyme in the free form (µmol min^{-1} mg^{-1}).

The experimental data were fitted through Lineweaver-Burk

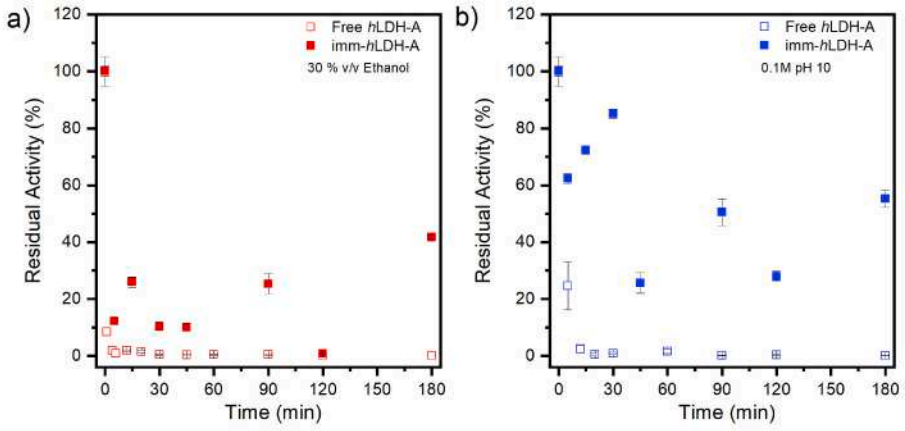

Fig. 13. Stability of hLDH-A free and best-immobilized when incubated in 30 % v/v ethanol solution (a) or carbonate buffer pH 10 (b) at room temperature for 3 h. The activity tests were carried out at 35 °C and pH 7.5. 59.

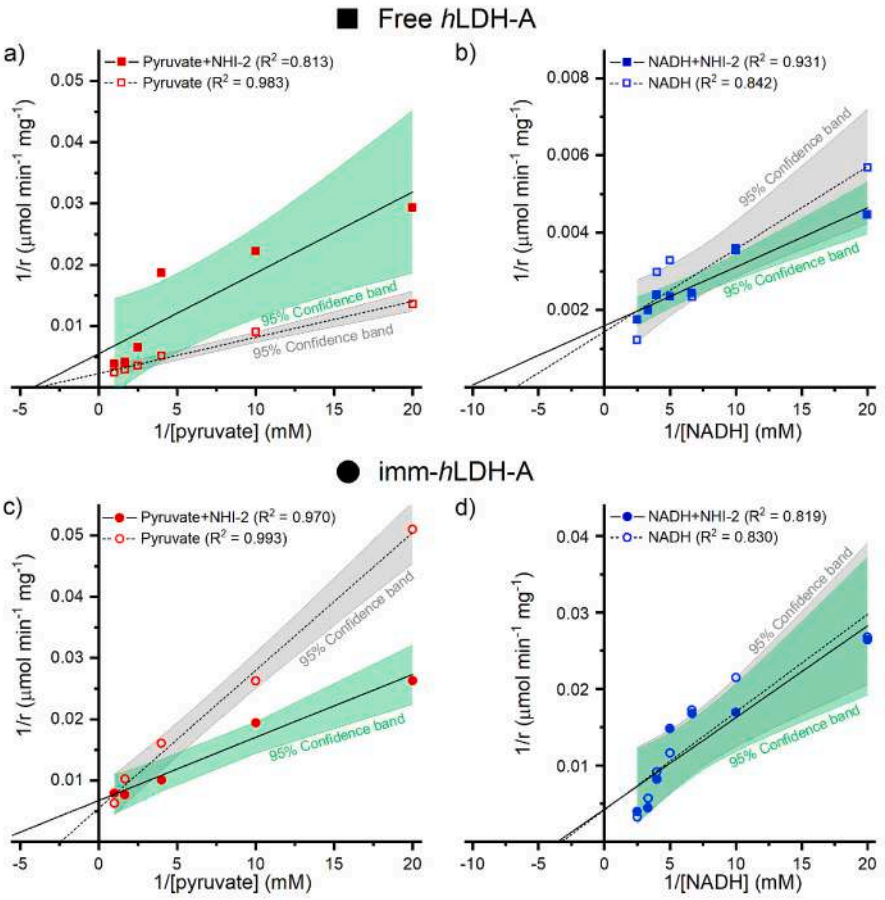

Fig. 14. Comparison of kinetic curves, linearized by Lineweaver-Burk methods, in the presence of NHI-2 (20 µM) by varying the concentration of pyruvate or NADH keeping the other reagent constant. The tests were repeated on the free enzyme and hLDH-A immobilized on mSBA-15. The tests were carried out at 35 °C and 0.1 M phosphate buffer pH 7.5. 60.

Table 5
hLDH-A apparent kinetic parameters obtained with the Lineweaver-Burk plots in the presence of 20 µM NHI-2 by varying the concentration of pyruvate or NADH.

Enzyme form	Limiting reagent	NHI-2	V_{max} (µmol min^{-1} mg^{-1})	K_{half} (mM)
Free	Pyruvate	No	442	0,26
		Yes	182	0,24
	NADH	No	694	0,15
		Yes	629	0,10
Immobilized on mSBA-15	Pyruvate	No	182	0,41
		Yes	148	0,15
	NADH	No	240	0,31
		Yes	234	0,28

linearization as shown in Fig. 14.

Table 5 reports the apparent kinetic parameters obtained via the Lineweaver-Burk plots. Additionally, employing a Michaelis-Menten model, the effectiveness factor for imm-*h*LDH-A was computed, and the results are visualized in Fig. S7 of the Supporting Information. The trend of the effectiveness factor, as depicted in Fig. S7a, suggests a lower pyruvate concentration within the silica pores compared to the bulk concentration, attributable to internal diffusional restrictions (IDR), causing a reduced rate compared to the soluble enzyme. In contrast, when NHI-2 is added to the solution, no diffusional restrictions are detected. This effect is likely due to the higher diffusional rate of the inhibitor than the reaction rate. Conversely, NADH presents similar IDR both in the presence or in the absence of NHI-2, as illustrated by the trend of the effectiveness factor shown in Fig. 7b. This observation seems to align with the findings reported in Table 5.

The apparent parameters seem to describe mixed-type inhibition mechanisms [68], in accordance with what was previously reported by Granchi et al. [69]. As described by Piumetti et al. [70], this type of inhibition is generally due to an allosteric effect which provokes a change in the structural conformation of the enzyme. Fig. 15 represents the enzymatic pocket of *h*LDH-A when the enzyme interacts with the cofactor and the substrate (Fig. 15a and b) and with the inhibitor (Fig. 15c and d), realized with BIOVIA Discovery Studio [71]. The amino acids implied in the interaction with pyruvate, NADH, and inhibitor are listed in Table S1.

As suggested by the simulation shown in Fig. 15, the inhibitor located in the enzymatic pocket can hamper the formation of the enzyme-substrate-cofactor complex. Moreover, it can be noted that the lysine residues are quite evenly distributed. From this graphical analysis it can be deduced that an improper covalent binding with the silica surface can cause an inactive biocatalyst or a partial alteration of the three-dimensional structure of the enzyme. The latter can explain the different variation of the apparent kinetic parameters obtained on imm-*h*LDH-A with respect to the free enzyme by varying the pyruvate concentrations.

4. Conclusions

The present research aimed to examine the use of three different mesoporous silicas as support for the enzyme *h*LDH-A in order to obtain a stable and durable LDH-based microreactor. This study has shown that the synthesis procedures adopted were effective in preparing

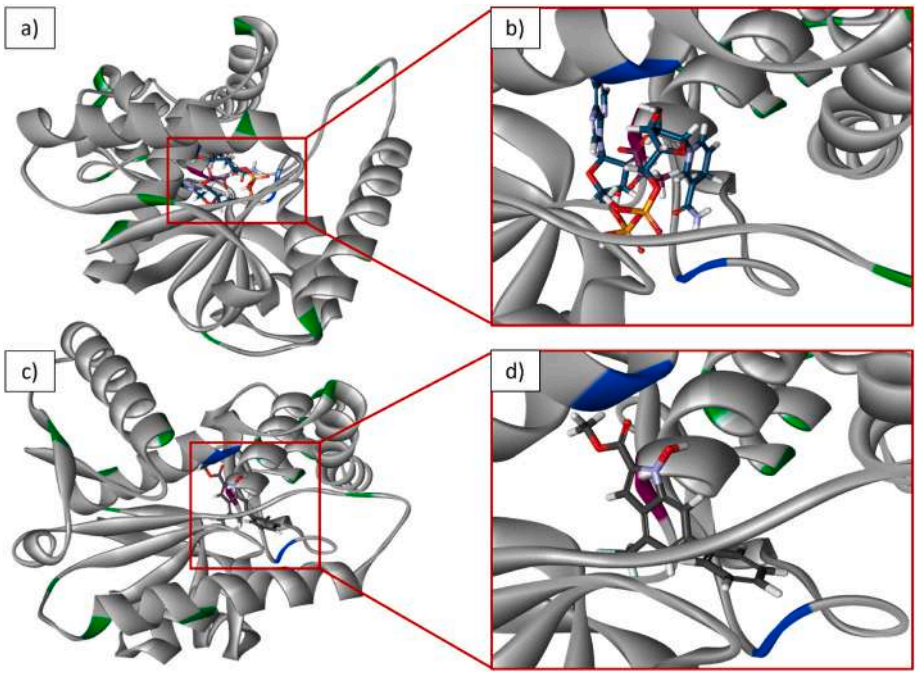

Fig. 15. Simulation results for hLDH-A complex with NADH and pyruvate (a) and magnification (b) and with the inhibitor NHI-2 (c) and magnification (d). The highlighted amino acid residues in the three-dimensional structure of hLDH-A are involved in interactions with the cofactor (blue) and pyruvate (purple). Moreover, the lysine residues implicated in the immobilization are depicted in green. The molecules of pyruvate, NADH, and NHI-2 were obtained from the PubChem online library while the hLDH-A three-dimensional structure was obtained from the AlphaFold Protein Structure Database. The simulation was performed by using BIOVIA Discovery Studio (DS) software. 61.

mesoporous silica with spongy-like networks and dendritic structure. With all the tested supports, immobilization yields higher than 80 % have been obtained. Overall, the retained activities were higher in the presence of trehalose used as a stabilizing agent than with PEG. The best result (R_{act} ~ 15 %) was achieved when mSBA-15 was used as support, which is probably due to a balanced number of functional groups, the less negative value of ζ-potential, and the morphology of this material which seems to cause fewer conformational changes of the enzyme and substrate diffusion related problems compared to MCF and DPS. The findings of this research suggest that this mesoporous silica used as support was successful in increasing the durability and stability of imm-*h*LDH-A with respect to the free form. This is demonstrated by the outcomes achieved from the inactivation tests. Indeed, after incubation in 30 % v/v ethanol and alkaline pH solutions, imm-*h*LDH-A has residual activities of 20 % and 35 % respectively, after 3 h of incubation. In contrast, the enzyme in the free form was completely inactivated after 5 min of incubation at the same conditions. Finally, the apparent kinetic parameters obtained through Lineweaver-Burk linearization in the presence of NHI-2 inhibitor seem to describe mixed-type inhibition mechanisms. Both in the free and immobilized enzyme forms, the reduction of the apparent V_{max} was higher when pyruvate concentration was varied and NADH concentration was kept constant and in excess. The results of this research support the idea that the covalent immobilization of enzymes on mesoporous silica is a viable strategy to increase the stability and durability of *h*LDH-A. Despite the evident improvements in stability and durability post-immobilization, there exists significant potential for further enhancing the activity of imm-*h*LDH-A. In fact, the covalent bonds formed between the enzyme and the support during the immobilization process might induce conformational changes or increase rigidity within the biomolecule, as suggested by the position of the lysine residues, (which is noticeable in the visual simulation) changing the response of the enzyme in the presence of NHI-2. Further research should focus on studying the conformation of the *h*LDH-A when immobilized on mesoporous silica for refining the immobilization process to optimize enzyme performance, and consequently a more precise measurement of its inhibition.

CRediT authorship contribution statement

Clarissa Cocuzza: Writing – review & editing, Writing – original draft, Investigation, Formal analysis, Data curation, Conceptualization. **Chiara Vincenzi:** Investigation. **Carminna Ottone:** Writing – review & editing, Supervision, Methodology, Formal analysis. **Andrés Illanes:** Writing – review & editing. **Debora Fino:** Funding acquisition. **Valentina Cauda:** Writing – review & editing, Investigation. **Marco Piumetti:** Writing – review & editing, Supervision, Project administration, Methodology.

Declaration of competing interest

The authors declare that they have no known competing financial interests or personal relationships that could have appeared to influence the work reported in this paper.

Data availability

Data will be made available on request.

Acknowledgements

Elena Antoniono and Veronica Li Volsi for the help given in data acquisition. Enrico Sartoretti for the acquisition of FESEM images and for the help to perform FT-IR analysis. Marco Allione for the acquisition of HR-TEM images. The authors acknowledge Politecnico di Torino for paying the APC fee.

Appendix A. Supplementary data

Supplementary data to this article can be found online at https://doi.org/10.1016/j.micromeso.2024.113182.

References

[1] Global Cancer Observatory - IARC, Cancer tomorrow. https://gco.iarc.fr/tomorrow/en/dataviz/isotype, 2020. (Accessed 29 December 2023).

[2] C. Cocuzza, E. Antoniono, C. Ottone, V. Cauda, D. Fino, M. Piumetti, Preparation of a mesoporous biosensor for lactate dehydrogenase (hLDH-A) as potential anticancer inhibitor screening, ACS Biomater. Sci. Eng. 9 (2023) 6045–6057, https://doi.org/10.1021/acsbiomaterials.3c00582.

[3] L. Ippolito, A. Morandi, E. Giannoni, P. Chiarugi, Lactate: a metabolic driver in the tumour landscape, Trends Biochem. Sci. 44 (2019) 153–166, https://doi.org/10.1016/j.tibs.2018.10.011.

[4] K.G. de la Cruz-López, L.J. Castro-Muñoz, D.O. Reyes-Hernández, A. García-Carrancá, J. Manzo-Merino, Lactate in the regulation of tumor microenvironment and therapeutic approaches, Front. Oncol. 9 (2019), https://doi.org/10.3389/fonc.2019.01143.

[5] K. Augoff, A. Hryniewicz-Jankowska, R. Tabola, Lactate dehydrogenase 5: an old friend and a new hope in the war on cancer, Cancer Lett. 358 (2015) 1–7, https://doi.org/10.1016/j.canlet.2014.12.035.

[6] R. Kusumawati, A.H. Nasrullah, R.N. Pesik, Muthmainah, D. Indarto, Secondary metabolites of Mirabilis jalapa structurally inhibit Lactate Dehydrogenase A in silico: a potential cancer treatment, in: IOP Conf. Ser. Mater. Sci. Eng., Institute of Physics Publishing, 2018, https://doi.org/10.1088/1757-899X/333/1/012078.

[7] S.L. Zhang, Y. He, K.Y. Tam, Targeting cancer metabolism to develop human lactate dehydrogenase (hLDH)5 inhibitors, Drug Discov. Today 23 (2018) 1407–1415, https://doi.org/10.1016/j.drudis.2018.05.014.

[8] L. Wang, Y. Song, H. Wang, X. Zhang, M. Wang, J. He, S. Li, L. Zhang, K. Li, L. Cao, Advances of artificial intelligence in anti-cancer drug design: a review of the past decade, Pharmaceuticals 16 (2023), https://doi.org/10.3390/ph16020253.

[9] W. Cui, A. Aouidate, S. Wang, Q. Yu, Y. Li, S. Yuan, Discovering anti-cancer drugs via computational methods, Front. Pharmacol. 11 (2020) 1–14, https://doi.org/10.3389/fphar.2020.00733.

[10] S. Arana-Peña, D. Carballares, R. Morellon-Sterling, J. Rocha-Martin, R. Fernandez-Lafuente, The combination of covalent and ionic exchange immobilizations enables the coimmobilization on vinyl sulfone activated supports and the reuse of the most stable immobilized enzyme, Int. J. Biol. Macromol. 199 (2022) 51–60, https://doi.org/10.1016/j.ijbiomac.2021.12.148.

[11] O. Barbosa, R. Torres, C. Ortiz, Á. Berenguer-Murcia, R.C. Rodrigues, R. Fernandez-Lafuente, Heterofunctional supports in enzyme immobilization: from traditional immobilization protocols to opportunities in tuning enzyme properties, Biomacromolecules 14 (2013) 2433–2462, https://doi.org/10.1021/bm400762h.

[12] A.M. Baracu, L.A. Dinu Gugoasa, Review—recent advances in microfabrication, design and applications of amperometric sensors and biosensors, J. Electrochem. Soc. 168 (2021) 037503, https://doi.org/10.1149/1945-7111/abe8b6.

[13] S. Tvorynska, J. Barek, B. Josypcuk, High-performance amperometric biosensor for flow injection analysis consisting of a replaceable lactate oxidase-based mini-reactor and a silver amalgam screen-printed electrode, Electrochim. Acta 445 (2023), https://doi.org/10.1016/j.electacta.2023.142033.

[14] N. Carlsson, H. Gustafsson, C. Thörn, L. Olsson, K. Holmberg, B. Åkerman, Enzymes immobilized in mesoporous silica: a physical-chemical perspective, Adv. Colloid Interface Sci. 205 (2014) 339–360, https://doi.org/10.1016/j.cis.2013.08.010.

[15] D. Alagöz, A. Toprak, N.E. Varan, D. Yildirim, S.S. Tükel, Effective immobilization of lactate dehydrogenase onto mesoporous silica, Biotechnol. Appl. Biochem. (2021) 1–11, https://doi.org/10.1002/bab.2304.

[16] D. Gößl, H. Singer, H.Y. Chiu, A. Schmidt, M. Lichtnecker, H. Engelke, T. Bein, Highly active enzymes immobilized in large pore colloidal mesoporous silica nanoparticles, New J. Chem. 43 (2019) 1671–1680, https://doi.org/10.1039/c8nj04585b.

[17] C. Bernal, L. Sierra, M. Mesa, Improvement of thermal stability of β-galactosidase from *Bacillus circulans* by multipoint covalent immobilization in hierarchical macro-mesoporous silica, J. Mol. Catal. B Enzym. 84 (2012) 166–172, https://doi.org/10.1016/j.molcatb.2012.05.023.

[18] G. Pietricola, T. Tommasi, M. Dosa, E. Camelin, E. Berruto, C. Ottone, D. Fino, V. Cauda, M. Piumetti, Synthesis and characterization of ordered mesoporous silicas for the immobilization of formate dehydrogenase (FDH), Int. J. Biol. Macromol. 177 (2021) 261–270, https://doi.org/10.1016/j.ijbiomac.2021.02.114.

[19] S. Hudson, J. Cooney, E. Magner, Proteins in mesoporous silicates, Angew. Chem. Int. Ed. 47 (2008) 8582–8594, https://doi.org/10.1002/anie.200705238.

[20] M. Piumetti, B. Bonelli, P. Massiani, S. Dzwigaj, I. Rossetti, S. Casale, L. Gaberova, M. Armandi, E. Garrone, Effect of vanadium dispersion and support properties on the catalytic activity of V-SBA-15 and V-MCF mesoporous materials prepared by direct synthesis, Catal. Today 176 (2011) 458–464, https://doi.org/10.1016/j.cattod.2010.10.066.

[21] M. Piumetti, B. Bonelli, P. Massiani, Y. Millot, S. Dzwigaj, L. Gaberova, M. Armandi, E. Garrone, Novel vanadium-containing mesocellular foams (V-MCF) obtained by direct synthesis, Microporous Mesoporous Mater. 142 (2011) 45–54, https://doi.org/10.1016/j.micromeso.2010.11.010.

[22] R. Narayan, U.Y. Nayak, A.M. Raichur, S. Garg, Mesoporous silica nanoparticles: a comprehensive review on synthesis and recent advances, Pharmaceutics 10 (2018) 1–49, https://doi.org/10.3390/pharmaceutics10030118.

[23] E. Camelin, O. Romero, M. Piumetti, C. Ottone, A. Illanes, D. Fino, Mechanisms of interaction among enzymes and supports, in: Nanomater. Biocatal., Elsevier, 2021, pp. 105–148, https://doi.org/10.1016/B978-0-12-824436-4.00022-8.

[24] P. Saengdee, W. Chaisriratanakul, W. Bunjongpru, W. Sripumkhai, A. Srisuwan, W. Jeamsaksiri, C. Hruanun, A. Poyai, C. Promptmas, Surface modification of silicon dioxide, silicon nitride and titanium oxynitride for lactate dehydrogenase immobilization, Biosens. Bioelectron. 67 (2015) 134–138, https://doi.org/10.1016/j.bios.2014.07.057.

[25] J.M. Guisan, J.M. Bolivar, F. López-Gallego, J. Rocha-Martín (Eds.), Immobilization of Enzymes and Cells Methods and Protocols, fourth ed., Humana Press, Hatfield, Hertfordshire, UK, 2010. http://www.springer.com/series/7651.

[26] P.C. Kuo, Z.X. Lin, T.Y. Wu, C.H. Hsu, H.P. Lin, T.S. Wu, Effects of morphology and pore size of mesoporous silicas on the efficiency of an immobilized enzyme, RSC Adv. 11 (2021) 10010–10017, https://doi.org/10.1039/d1ra01358k.

[27] B. Zhou, N. Qi, B. Wang, Z.Q. Chen, Effect of swelling agent on the pore structure of SBA-15 studied by positron annihilation, Appl. Surf. Sci. 475 (2019) 961–968, https://doi.org/10.1016/j.apsusc.2019.01.056.

[28] S.G. Kothalawala, J. Jiao, R. Speight, H. Song, Y. Yang, J. Zhang, Pore architecture influences the enzyme immobilization performance of mesoporous silica nanospheres, Microporous Mesoporous Mater. 338 (2022) 111963, https://doi.org/10.1016/j.micromeso.2022.111963.

[29] H. Chen, H. Liu, R. Wang, X. Jiang, M. Zhu, Size-controllable synthesis of dendritic porous silica as reinforcing fillers for dental composites, Dent. Mater. 37 (2021) 961–971, https://doi.org/10.1016/j.dental.2021.02.015.

[30] C. Cocuzza, G. Pietricola, I. Zonca, M. Dosa, O. Romero, T. Tommasi, V. Cauda, D. Fino, C. Ottone, M. Piumetti, Simultaneous CO 2 reduction and NADH regeneration using formate and glycerol dehydrogenase enzymes co-immobilized on modified natural zeolite, RSC Adv. 12 (2022) 31142–31155, https://doi.org/10.1039/d2ra03459j.

[31] M. Piumetti, M. Armandi, E. Garrone, B. Bonelli, An IR spectroscopy assessment of the surface acidity of mesoporous VO x-SiO 2 catalysts, Microporous Mesoporous Mater. 164 (2012) 111–119, https://doi.org/10.1016/j.micromeso.2012.05.041.

[32] B. Bonelli, M. Cozzolino, R. Tesser, M. Di Serio, M. Piumetti, E. Garrone, E. Santacesaria, Study of the surface acidity of TiO2/SiO2 catalysts by means of FTIR measurements of CO and NH3 adsorption, J. Catal. 246 (2007) 293–300, https://doi.org/10.1016/j.jcat.2006.12.015.

[33] H.P. Erickson, Size and shape of protein molecules at the nanometer level determined by sedimentation, gel filtration, and electron microscopy, Biol. Proced. Online 11 (2009) 32–51, https://doi.org/10.1007/s12575-009-9008-x.

[34] J.M. Guisan, G. Fernandez-Lorente, J. Rocha-Martin, D. Moreno-Gamero, Enzyme immobilization strategies for the design of robust and efficient biocatalysts, Curr. Opin. Green Sustainable Chem. 35 (2022) 100593, https://doi.org/10.1016/j.cogsc.2022.100593.

[35] S.R. Patel Yusdy, M.G.S. Yap, D.I.C. Wang, Immobilization of l-lactate dehydrogenase on magnetic nanoclusters for chiral synthesis of pharmaceutical compounds, Biochem. Eng. J. 48 (2009) 13–21, https://doi.org/10.1016/j.bej.2009.07.017.

[36] E. Jackson, F. López-Gallego, J.M. Guisan, L. Betancor, Enhanced stability of L-lactate dehydrogenase through immobilization engineering, Process Biochem. 51 (2016) 1248–1255, https://doi.org/10.1016/j.procbio.2016.06.001.

[37] J. Boudrant, J.M. Woodley, R. Fernandez-Lafuente, Parameters necessary to define an immobilized enzyme preparation, Process Biochem. 90 (2020) 66–80, https://doi.org/10.1016/j.procbio.2019.11.026.

[38] J. Rocha-Martín, B. de Las Rivas, R. Muñoz, J.M. Guisán, F. López-Gallego, Rational co-immobilization of bi-enzyme cascades on porous supports and their applications in bio-redox reactions with insitu recycling of soluble cofactors, ChemCatChem 4 (2012) 1279–1288, https://doi.org/10.1002/cctc.201200146.

[39] G. Pietricola, T. Tommasi, M. Dosa, E. Camelin, E. Berruto, C. Ottone, D. Fino, V. Cauda, M. Piumetti, Synthesis and characterization of ordered mesoporous silicas for the immobilization of formate dehydrogenase (FDH), Int. J. Biol. Macromol. 177 (2021) 261–270, https://doi.org/10.1016/j.ijbiomac.2021.02.114.

[40] R.M. Pasternack, S.R. Amy, Y.J. Chabal, Attachment of 3-(aminopropyl) triethoxysilane on silicon oxide surfaces: dependence on solution temperature, Langmuir 24 (2008) 12963–12971, https://doi.org/10.1021/la8024827.

[41] M. Thommes, K.A. Cychosz, Physical adsorption characterization of nanoporous materials: progress and challenges, Adsorption 20 (2014) 233–250, https://doi.org/10.1007/s10450-014-9606-z.

[42] M. Thommes, K. Kaneko, A.V. Neimark, J.P. Olivier, F. Rodriguez-Reinoso, J. Rouquerol, K.S.W. Sing, Physisorption of gases, with special reference to the evaluation of surface area and pore size distribution (IUPAC Technical Report), Pure Appl. Chem. 87 (2015) 1051–1069, https://doi.org/10.1515/pac-2014-1117.

[43] J.O. Otalvaro, M. Avena, M. Brigante, Adsorption of organic pollutants by amine functionalized mesoporous silica in aqueous solution. Effects of pH, ionic strength and some consequences of APTES stability, J. Environ. Chem. Eng. 7 (2019) 103325, https://doi.org/10.1016/j.jece.2019.103325.

[44] M.C. Ruiz-Cañas, L.M. Corredor, H.I. Quintero, E. Manrique, A.R. Romero Bohórquez, Morphological and structural properties of amino-functionalized fumed nanosilica and its comparison with nanoparticles obtained by modified Stöber method, Molecules 25 (2020), https://doi.org/10.3390/molecules25122868.

[45] S. Fiorilli, D. Caldarola, H. Ma, B. Onida, Bi-functionalization of silica spheres with sulfonic and carboxylic groups via a co-condensation route, J. Sol. Gel Sci. Technol. 60 (2011) 260–265, https://doi.org/10.1007/s10971-011-2484-x.

[46] S. Fiorilli, B. Onida, B. Bonelli, E. Garrone, In situ infrared study of SBA-15 functionalized with carboxylic groups incorporated by a Co-condensation route, J. Phys. Chem. B 109 (2005) 16725–16729, https://doi.org/10.1021/jp045362y.

[47] D. Caldarola, D.P. Mitev, L. Marlin, E.P. Nesterenko, B. Paull, B. Onida, M. C. Bruzzoniti, R.M. De Carlo, C. Sarzanini, P.N. Nesterenko, Functionalisation of mesoporous silica gel with 2-[(phosphonomethyl)-amino] acetic acid functional groups. Characterisation and application, Appl. Surf. Sci. 288 (2014) 373–380, https://doi.org/10.1016/j.apsusc.2013.10.035.

[48] C. Vittoni, G. Gatti, G. Paul, E. Mangano, S. Brandani, C. Bisio, L. Marchese, Non-porous versus mesoporous siliceous materials for CO2 capture, ChemistryOpen 8 (2019) 719–727, https://doi.org/10.1002/open.201900084.
[49] C. Yang, H. Su, G. Du, X. Ren, Y. Wu, H. Zhang, K. Ni, X. Ran, J. Li, W. Gao, L. Yang, Aldehyde-amine crosslinked starch-based high-performance wood adhesive, Eur. J. Wood Wood Prod. 81 (2023) 1557–1568, https://doi.org/10.1007/s00107-023-01985-w.
[50] K. Bouchmella, Q. Lion, C. Gervais, M.B. Cardoso, Impact of mesoporous silica functionalization fine-tuning on antibiotic uptake/delivery and bactericidal activity, ACS Omega 8 (2023) 12154–12164, https://doi.org/10.1021/acsomega.2c08065.
[51] S. Nazari, M. Gholami, M. Farzadkia, F. Akbari Dourbash, M. Arzanlou, R. R. Kalantary, Synthesis and evaluation of the antibacterial effect of silica-coated modified magnetic poly-(amidoamine) G5 nanoparticles on E. coli and S. aureus, J. Mol. Liq. 276 (2019) 93–104, https://doi.org/10.1016/j.molliq.2018.11.101.
[52] G.S. Foo, J.J. Lee, C.H. Chen, S.E. Hayes, C. Sievers, C.W. Jones, Elucidation of surface species through in situ FTIR spectroscopy of Carbon dioxide adsorption on amine-grafted SBA-15, ChemSusChem 10 (2017) 266–276, https://doi.org/10.1002/cssc.201600809.
[53] N. Majoul, S. Aouida, B. Bessaïs, Progress of porous silicon APTES-functionalization by FTIR investigations, Appl. Surf. Sci. 331 (2015) 388–391, https://doi.org/10.1016/j.apsusc.2015.01.107.
[54] S.N. Rahaman, S. Pathmanapan, A. Sidharthan, S.K. Anandasadagopan, Vancomycin loaded amino-functionalized MCM-48 mesoporous silica nanoparticles as a promising drug carrier in bone substitutes for bacterial infection management, Appl. Biochem. Biotechnol. (2023) 6607–6632, https://doi.org/10.1007/s12010-023-04406-z.
[55] J. Gajardo, J. Colmenares-Zerpa, A.F. Peixoto, D.S.A. Silva, J.A. Silva, F. Gispert-Guirado, J. Llorca, E.A. Urquieta-Gonzalez, J.B.O. Santos, J. Szanyi, C. Sepúlveda, M.G. Álvarez, R.J. Chimentão, Revealing the effects of high Al loading incorporation in the SBA-15 silica mesoporous material, J. Porous Mater. 30 (2023) 1687–1707, https://doi.org/10.1007/s10934-023-01453-z.
[56] V. Degirmenci, D. Uner, B. Cinlar, B.H. Shanks, A. Yilmaz, R.A. Van Santen, E.J. M. Hensen, Sulfated zirconia modified SBA-15 catalysts for cellobiose hydrolysis, Catal. Lett. 141 (2011) 33–42, https://doi.org/10.1007/s10562-010-0466-1.
[57] Z. Chen, F.C. Hsu, D. Battigelli, H.C. Chang, Capture and release of viruses using amino-functionalized silica particles, Anal. Chim. Acta 569 (2006) 76–82, https://doi.org/10.1016/j.aca.2006.03.103.
[58] N.I. Sabeela, T.M. Almutairi, H.A. Al-Lohedan, A.O. Ezzat, A.M. Atta, Reactive mesoporous ph-sensitive amino-functionalized silica nanoparticles for efficient removal of coomassie blue dye, Nanomaterials 9 (2019), https://doi.org/10.3390/nano9121721.
[59] Y. Wang, F. Caruso, Mesoporous silica spheres as supports for enzyme immobilization and encapsulation, Chem. Mater. 17 (2005) 953–961, https://doi.org/10.1021/cm0483137.
[60] J.K. Kaushik, R. Bhat, Why is trehalose an exceptional protein stabilizer? An analysis of the thermal stability of proteins in the presence of the compatible osmolyte trehalose, J. Biol. Chem. 278 (2003) 26458–26465, https://doi.org/10.1074/jbc.M300815200.
[61] A.M. Basso, B.P. Nicola, K. Bernardo-Gusmão, S.B.C. Pergher, Tunable effect of the calcination of the silanol groups of KIT-6 and SBA-15 mesoporous materials, Appl. Sci. 10 (2020) 1–16, https://doi.org/10.3390/app10030970.
[62] J. Boudrant, J.M. Woodley, R. Fernandez-Lafuente, Parameters necessary to define an immobilized enzyme preparation, Process Biochem. 90 (2020) 66–80, https://doi.org/10.1016/j.procbio.2019.11.026.
[63] M. Carbonaro, A. Nucara, Secondary structure of food proteins by Fourier transform spectroscopy in the mid-infrared region, Amino Acids 38 (2010) 679–690, https://doi.org/10.1007/s00726-009-0274-3.
[64] M. Hiraoui, M. Guendouz, N. Lorrain, A. Moadhen, L. Haji, M. Oueslati, Spectroscopy studies of functionalized oxidized porous silicon surface for biosensing applications, Mater. Chem. Phys. 128 (2011) 151–156, https://doi.org/10.1016/j.matchemphys.2011.02.052.
[65] R.C. Rodrigues, Á. Berenguer-Murcia, D. Carballares, R. Morellon-Sterling, R. Fernandez-Lafuente, Stabilization of enzymes via immobilization: multipoint covalent attachment and other stabilization strategies, Biotechnol. Adv. 52 (2021) 107821, https://doi.org/10.1016/j.biotechadv.2021.107821.
[66] A. Illanes, R. Fernández-Lafuente, J.M. Guisán, L. Wilson, Heterogeneous enzyme kinetics, in: Enzym. Biocatal. Princ. Appl., Springer, Dordrecht, 2008, pp. 155–203, https://doi.org/10.1007/978-1-4020-8361-7_4.
[67] C. Bahamondes, G. Álvaro, L. Wilson, A. Illanes, Effect of enzyme load and catalyst particle size on the diffusional restrictions in reactions of synthesis and hydrolysis catalyzed by α-chymotrypsin immobilized into glyoxal-agarose, Process Biochem. 53 (2017) 172–179, https://doi.org/10.1016/j.procbio.2016.12.004.
[68] B. Das, R. Yan, A close look at BACE1 inhibitors for alzheimer's disease treatment, CNS Drugs 33 (2019) 251–263, https://doi.org/10.1007/s40263-019-00613-7.
[69] C. Granchi, E.C. Calvaresi, T. Tuccinardi, I. Paterni, M. Macchia, A. Martinelli, P. J. Hergenrother, F. Minutolo, Assessing the differential action on cancer cells of LDH-A inhibitors based on the N-hydroxyindole-2-carboxylate (NHI) and malonic (Mal) scaffolds, Org. Biomol. Chem. 11 (2013) 6588–6596, https://doi.org/10.1039/c3ob40870a.
[70] M. Piumetti, A. Illanes, Enzymes and their function, in: Mol. Dyn. Complex. Catal. Biocatal., Springer International Publishing, Cham, 2022, pp. 23–53, https://doi.org/10.1007/978-3-030-88500-7_2.
[71] Dassault Systems, BIOVIA, Discovery Studio Modeling Environment, 2020.